



Liquefaction Resistance and Cyclic Response of Air Injected-Desaturated Sandy Soil

Dhanaji Chavan · Thallak G. Sitharam · P. Anbazhagan

Received: 3 April 2020 / Accepted: 20 September 2021 / Published online: 29 September 2021
© The Author(s), under exclusive licence to Springer Nature Switzerland AG 2021

Abstract Desaturation of in-situ saturated sandy soils is emerging as a new cost effective and environment friendly liquefaction mitigation technique. In the present study, stress controlled undrained cyclic triaxial tests have been conducted on air injected-desaturated sandy soil and various important issues such as number of cycles required for initial liquefaction, cyclic strength of desaturated sand, modes of failure, evolution of pore pressure, have been explored in detail. Number of cycles required for initial liquefaction increased exponentially with decrease in degree of saturation. Cyclic strength of desaturated sand with degree of saturation of 80% is found to be twice that of saturated sand, for relative density of 40%. Assessment of performance of desaturated sand under various earthquake records revealed that desaturated sand with degree of saturation of 70% can prevent liquefaction during moderate to strong earthquakes having peak ground acceleration as high as 0.30 g. Further, sample with high degree of saturation underwent cyclic mobility failure. In samples with low degree of saturation, two types of cyclic softening failures demarcated by two distinct phase transformation trends were

observed. A pore pressure model proposed by Konstantinou and Georgiannou (2014) has been modified to predict the pore pressure evolution in desaturated sand.

Keywords Air injection · Desaturation · Initial liquefaction · Cyclic mobility · Pore pressure ratio

Abbreviations

a_{max}	Peak horizontal acceleration at the ground surface;
B	Skempton's pore pressure parameter;
D_r	Relative density of the sample;
g	Gravitational acceleration;
K_s	Bulk modulus of soil skeleton;
K_w	Bulk modulus of water;
N	Number of loading cycles;
N_i	Number of cycles required for initial liquefaction;
n	Porosity of the sample;
p'	Effective mean stress;
q	Deviatoric stress;
r_u	Pore pressure ratio;
S	Degree of saturation of the sample;
u_a	Absolute pore fluid pressure;
σ'_c	Effective confining pressure at the end of consolidation;
σ_v	Total vertical pressure;
σ'_v	Effective vertical pressure

D. Chavan (✉) · T. G. Sitharam · P. Anbazhagan
Department of Civil Engineering, Indian Institute of Science, Bangalore 560012, India
e-mail: dschavan83@gmail.com

T. G. Sitharam
e-mail: sitharam@iisc.ac.in

P. Anbazhagan
e-mail: anbazhagan@iisc.ac.in

1 Introduction

Liquefaction of the soil has been one of the challenging areas of research in the field of geotechnical earthquake engineering. Over period of time many techniques such as deep dynamic compaction, compaction grouting, explosive compaction, deep soil mixing etc. have evolved as effective means to check the liquefaction of the soil (Idriss and Boulanger, 2008).

Over the last couple of years, induced desaturation of soil has been emerging as a new cost effective and environment friendly liquefaction mitigation technique (Ishihara et al. 2003; Pietruszczak et al. 2003; Yegian et al. 2007; Takemura et al. 2009; Zeybek and Madabhushi 2016, 2017a, b). In this technique air/gas is injected/generated into the originally saturated sandy soil (Okamura et al. 2011; He et al. 2013). The presence of air in the voids makes pore fluid compressible (Kokusho 2000; Okamura and Soga 2006). This, in turn, enhances the liquefaction resistance of the soil.

Shaking table and Centrifuge studies carried out on desaturated sandy soils had shown that initial liquefaction was prevented in such soils (Yegian et al. 2007; He et al. 2013). Furthermore, significant reduction in the settlement of shallow footings resting on desaturated sandy soils had also been observed (Takemura et al. 2009; Marasini and Okamura 2015a, b; Zeybek and Madabhushi 2016). He et al. (2014), performed monotonic undrained triaxial tests on microbially desaturated loose clean sand and found that reduction in the degree of saturation even by 5 to 10% doubled the undrained shear strength of the soil.

Zeybek and Madabhushi (2017a) assessed durability of the entrapped air bubbles under hydrostatic, upward and downward flow and lateral shaking and found that there was very small change in the degree of saturation. Similar study was conducted by Esellerbayat et al. (2013). They found that under hydrostatic condition, degree of saturation increased from 82% to 84% over the period of 115 weeks (i.e., 2.4 years). Further, they subjected specimens to upward hydraulic gradient in the range of 0.01 and 0.52 and observed that degree of saturation remained unaltered during upward flow. Zeybek et al. (2020) performed dynamic centrifuge tests on models comprising shallow footings resting on air desaturated sand beds. It was observed that footings resting on the saturated sand

bed underwent excessive settlements in comparison with those resting on desaturated sand bed.

Marasini and Okamura (2015b) simulated centrifuge models of shallow footings resting on desaturated sand bed employing coupled finite element program LIQCA-2D. It was inferred that desaturation was effective to mitigate liquefaction. Kato and Nagao (2020) simulated a series of large shaking table tests for saturated and desaturated condition employing software LIQCA2D17. The degree of saturation was in the range of 80% to 100%. It was found that pore pressure dissipation and volumetric strain altered the degree of saturation, during shaking.

Though noteworthy research has been carried out, in past, on liquefaction resistance of desaturated sandy soil, some of the important issues such as: (1) modes of failure of desaturated sandy soil subjected to cyclic loading (2) relationship between the number of cycles required for initial liquefaction and degree of saturation (3) cyclic strength (4) effect of desaturation on evolution of the pore pressure (5) assessment of performance of desaturated sand under various earthquake records, are yet to be explored.

To the authors' knowledge, present study is the first attempt to desaturate the triaxial specimen by air injection and performing cyclic triaxial tests on air injected-desaturated triaxial specimens.

In the present study, a systematic experimental investigation has been carried out to understand abovementioned issues. The degree of saturation considered in the present study varies from 70% to 99%, as this represents the degree of saturation achieved in field by air injection desaturation technique (Okamura et al. 2011). Tests have been conducted at effective confining pressures of 50 kPa and 100 kPa; and relative densities of 30%, 40% and 60%. The stress controlled undrained cyclic triaxial tests have been conducted with a sinusoidal loading having frequency of 0.1 Hz and cyclic shear stress ratio (*CSR*) of 0.175, 0.250, 0.300 and 0.400.

2 Material Used

The original sand was collected from bed of Sabarmati river near IIT Gandhinagar campus, Gujarat (India). Fraction of the sand passing through 2 mm IS sieve and retained on 75 micron IS sieve has been used in the present study. The gradation curve for this sand is shown

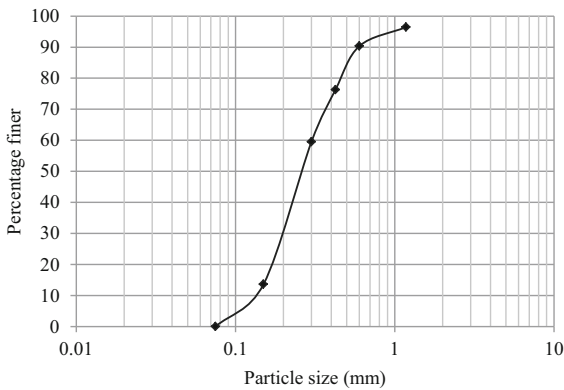


Fig. 1 Gradation curve of sand used in the present study

in the Fig. 1. It is poorly graded sand with coefficient of uniformity (C_u) 2.14 and coefficient of curvature (C_c) 0.95. Other characteristics of the sand used in this study have been given in the Table 1. Further, the scanning electron microscope (SEM) image of the sand at two different resolutions is shown in Fig. 2. It is observed that most of the particles are angular.

3 Experimental Program

3.1 Sample Preparation

The sample (50 mm diameter × 100 mm height) was prepared by dry deposition method, which is one of the

Table 1 Index properties of the sand used in the present study

G_s	e_{max}	e_{min}	ρ_{max} (gm/cc)	ρ_{min} (gm/cc)	D_{10} (mm)	D_{30} (mm)	D_{50} (mm)	D_{60} (mm)	C_u	C_c
2.65	0.84	0.45	1.83	1.44	0.14	0.20	0.27	0.30	2.14	0.95

most widely used methods (Ishihara 1996; Sze and Yang 2014; Xin et al. 2016), using a split mould. Oven dried mass of sand was deposited into the sample preparation mould in five layers. To deposit sand mass a funnel with spout was used. Throughout the deposition, drop height was maintained to be zero. After each layer little tamping was done with the help of funnel spout. At the end of the fifth layer little side tapping was also done.

3.2 Saturation of the Sample

To begin with, two different methods of saturation were tried. In the first method CO_2 gas was passed through the sample for 30 minutes followed by percolation of 1000 ml of distilled water. This is one of the conventional methods adopted to saturate the sample (Lade 2016). The degree of saturation achieved at the end of water percolation was found to be around 98%. This much high degree of saturation was achieved because sample was made of clean sand. To further increase the degree of saturation, back pressure of around 350 to 400 kPa was applied. On the application of this much high back pressure, the degree of saturation achieved was around 99%. It was also observed that keeping the sample under a back pressure of 400 kPa for even 3 days did not cause any further increase in the degree of saturation. It is worth

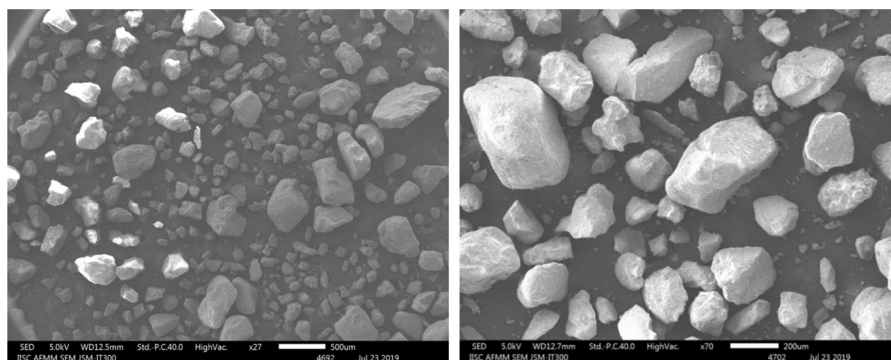


Fig. 2 Scanning Electron Microscope image of sand used in this study at two different resolutions

to note that a back pressure in the range of 700 kPa–1400 kPa is usually required to achieve full saturation of the sample when adopted conventional method (Rees 2017; ASTM:D5311/D5311M-13 2013; Lade 2016).

In the second method, CO₂ gas was passed in two stages: a) under a vacuum of 20 kPa for 10 minutes b) without vacuum for next 20 minutes (total 30 minutes), followed by percolation of 1000 ml of distilled water. It was observed that the degree of saturation achieved by second method was as high as 99%. Similar approach was adopted by Rad and Clough (1984) to saturate the sample at low back pressure. Black and Lee (1973) suggested that a sample with *S* of 99% can be considered as fully saturated sample from practical point of view. Therefore, in the present study, sample with *S* of 99% has been considered as a fully saturated sample. Further, for all the experiments in this study, second method was adopted to saturate the sample.

3.3 Desaturation of the Sample

Once the full saturation of the sample was ensured, a pipe supplying back pressure was disconnected from the back pressure valve at base of the triaxial cell and was replaced with a pipe supplying air as shown in Fig. 3a. Air under a very small pressure of around 2 kPa was injected into the sample from the base of the triaxial cell as shown in Fig. 3a. As air went in, it started pushing pore water out. The pore water coming out was collected in a small cup from the drainage valve as shown in Fig. 3b. Once the desired quantity of water was collected, air supply was stopped and drainage valve was closed. Then air supply pipe was replaced with the back pressure pipe. This back pressure pipe contained water at pressure of around 2 kPa. Next, back pressure valve was opened so that water from back pressure pipe could go in under small pressure of around 2 kPa. This condition was maintained for 10 minutes so that water and air could get adjusted in the sample. Next, Skempton's pore pressure parameter *B* was measured in conventional way and from that degree of saturation was computed as discussed in next section.

3.4 Selection of the Air Injection Pressure

It was suggested by Ishihara et al., (2003), from their centrifuge studies, that to inject the air into the saturated soil mass, the air injection pressure at the injection point has to be around 1.4 times the hydrostatic pressure at that point. Further, it was found by Okamura et al., (2011), from in-situ desaturation, that air started flowing into the soil mass when air injection pressure exceeded 1.1 times hydrostatic pressure at the injection point.

It should be noted here that initial pore water pressure in the triaxial specimen in the present study was just equal to hydrostatic pressure, as samples were saturated at zero back pressure, employing the second method discussed in Sect. 3.2. The height of the specimen in the present study is 100 mm. Therefore, the hydrostatic pressure at the base of the sample was just 1 kPa (i.e., 0.1 m height × 9.81). Further, as per the findings of Ishihara et al., (2003) and Okamura et al., (2011), air injection pressure required to desaturate triaxial specimen in the present study should be greater than 1.1 kPa. Therefore, in the present study air injection pressure was kept greater than 1.1 kPa (around 2 kPa).

3.5 Hydraulic Gradient During Desaturation

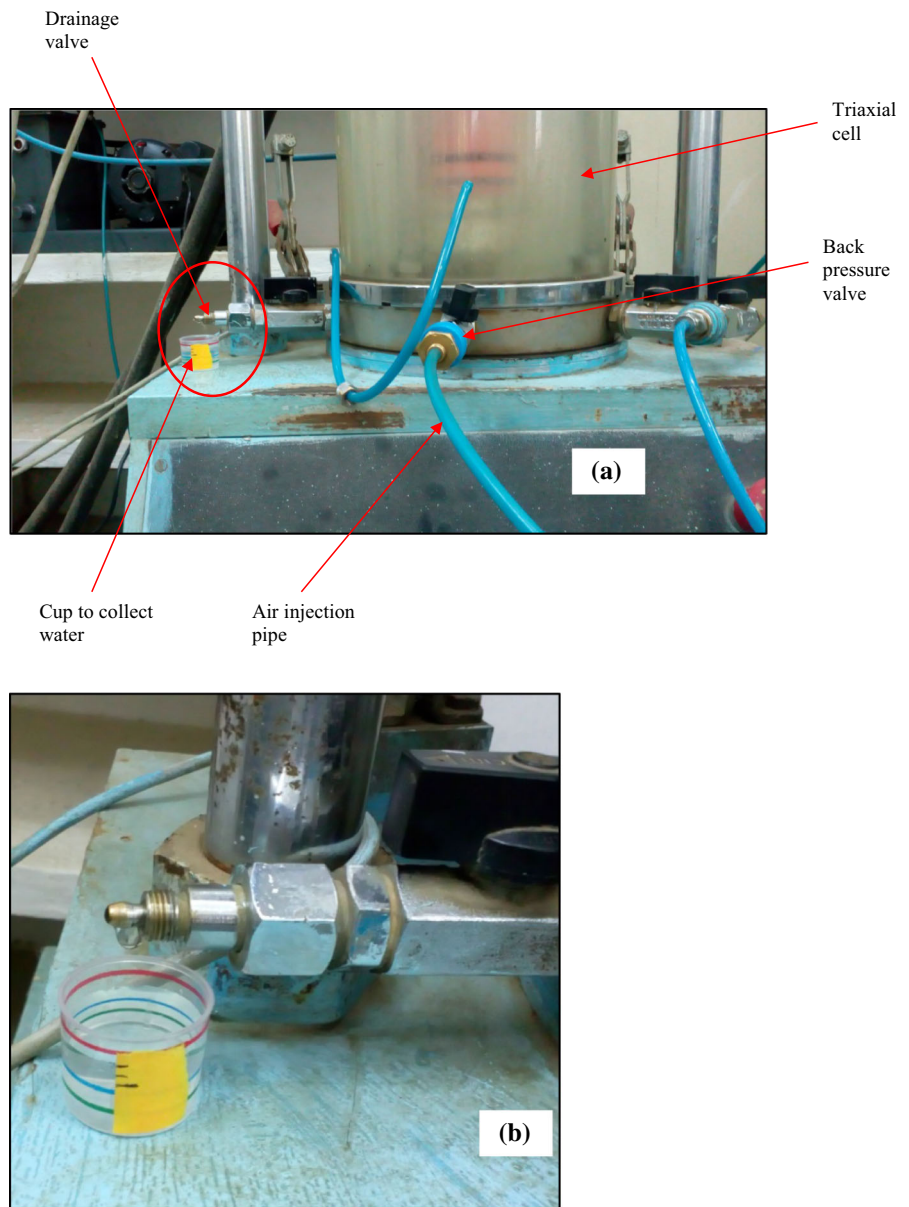
Initial pore water pressure in the specimen was 1 kPa. Air was injected at around 2 kPa. Thus, there was hydraulic head, $\Delta h = 2 - 1 = 1$ kPa. It should be noted that 1 kPa of hydraulic head is equivalent to 0.1 m height of water column. The specimen height is 0.1 m. This implies that there was hydraulic gradient of $\Delta h/L = 0.1/0.1 = 1$. This hydraulic gradient was responsible for the injection of air into the specimen.

3.5.1 Computation of the Degree of Saturation (*S*)

In the present study degree of saturation of the sample has been computed from Eq. (1), which had been widely used by other researchers as well (Sherif et al. 1977; Yoshimi et al. 1989; ; Ishihara et al. 2001a, b; Yang et al. 2004; Celestino and Kenneth 2012).

$$B = \left(\frac{1}{1 + nK_s[S/K_w + (1 - S)/u_a]} \right) \quad (1)$$

Fig. 3 Desaturation of the triaxial sample: **a** triaxial cell along with air injection pipe **b** enlarged view of encircled part (water collection) from figure (a)



where, B is Skempton’s pore pressure parameter which is defined as $\Delta u/\Delta\sigma_c$ (Skempton 1954), u_a is the absolute pore fluid pressure (i.e., atmospheric pressure + back pressure + Δu) at the end of cell pressure increment $\Delta\sigma_c$ (Lade 2016), S is the degree of saturation of the sample, n is the porosity of the sample, K_s is the bulk modulus of the soil skeleton, K_w is the bulk modulus of the pore water (2.23×10^6 kPa). Further, K_s was determined from the isotropic compression of the saturated specimen.

Values of K_s for relative densities used in this study are given in Table 2. It should be noted that above mentioned values are consistent with the values recorded in the literature for clean sands with dry density and index properties close to present study (Sherif et al. 1977).

Determination of Bulk modulus (K_s) of soil skeleton: Bulk modulus of the soil skeleton is given by $K = \Delta\sigma'_3/\Delta\varepsilon_v$, where σ'_3 is the isotropic effective confining pressure and ε_v is the volumetric strain (Lade

Table 2 Bulk modulus of samples of various densities

Relative density (D_r)	Void ratio (e)	Porosity (n)	Dry density (ρ_d) (gm/cc)	Bulk modulus (K_s) (kPa)
30	0.723	0.419	1.54	7.8×10^3
40	0.684	0.406	1.57	1.0×10^4
60	0.606	0.377	1.65	1.2×10^4

2016). The procedure adopted for the determination of bulk modulus in the present study is elaborated below:

For relative density of 40%: Sample was saturated by applying back pressure of 350 kPa. The corresponding cell pressure was 370 kPa. It should be noted that while applying back pressure, care was taken to maintain difference between cell pressure and back pressure to be 20 kPa. In other words, effective confining pressure of 20 kPa was maintained throughout. Once sample was saturated i.e., B parameter above 0.93, then cell pressure was slowly increased to 450 kPa keeping the drainage valve open. This resulted in drainage of 1.50 cm^3 of pore water. In other words, when cell pressure was increased from 370 to 450 kPa, specimen volume got changed by 1.50 cm^3 . The initial volume of the specimen was 196.35 cm^3 . Initial effective confining pressure was 20 kPa (370 kPa – 350 kPa), final effective confining pressure was 100 kPa (450 kPa – 350 kPa). Thus, increment in isotropic confining pressure $\Delta\sigma'_3$ of 80 kPa (100–20) was associated with a change in the volumetric strain $\Delta\varepsilon_v$ of 0.006213. This implies that bulk modulus of soil is 1.0×10^4 kPa. Similar approach was adopted for relative density of 30% and 60%.

In the present study, B -parameter has been measured at two instants: 1) during saturation 2) after desaturation. The degree of saturation corresponding to measured B -parameter was then computed from Eq. (1).

3.5.2 Verification of Eq. 1

In the present study, few tests were also conducted to determine degree of saturation S from measurement of water content w . The purpose behind these tests was to assess the accuracy of the degree of saturation S obtained from Eq. (1). In Fig. 4, the degree of saturation obtained from Eq. (1) is compared with that obtained from measurement of water content w . There is reasonably well agreement between S obtained from Eq. (1) and that from water content. This finding

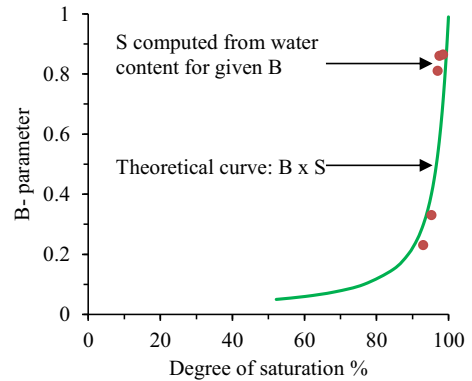


Fig. 4 Verification of S obtained from Eq. (1) with S obtained from water content (D_r 40%)

supports the use of Eq. (1) to obtain degree of saturation from Skempton's pore pressure parameter B .

3.6 Application of the Cyclic Loading

In this study, stress controlled undrained cyclic triaxial tests have been conducted using a servo controlled cyclic triaxial test set up at IISc Bangalore. A sinusoidal load with a frequency of 0.1 Hz was applied to the sample. Tests were conducted at cyclic stress ratio (CSR) of 0.175, 0.250, 0.300 and 0.400. CSR is the ratio of maximum cyclic shear stress and initial effective confining pressure. Initial effective confining pressure used in the study was 50 kPa and 100 kPa.

4 Desaturation and Initial liquefaction

4.1 Quantity of Water Ejected Versus Degree of Saturation

Air injected into the specimen pushes the pore water out. The amount of water ejected depends upon the amount of air injected into the specimen which

Table 3 Volume of water ejected and corresponding degree of saturation

Relative density D_r %	Volume of water ejected (ml)	Degree of saturation (S) %
30	2.5	97.0
	5	94.4
	5.5	94.1
	7	91.9
	11	86.6
	12	87.2
40	2.5	96.6
	5	93.1
	5.5	92.4
	9	88.6
	13.5	81.4
	19	69.2
60	4	94.1
	6	91.9
	11.5	83.6

depends on time period for which air injection is continued. Typical values of quantity of water ejected and corresponding degrees of saturation are mentioned in Table. 3. When 2.5 ml of water was ejected it resulted into S of 97% and 96.6% for sample of D_r 30% and 40%, respectively. From Table 3 it can be observed that higher the relative density, smaller is quantity of ejected water to achieve the same degree of saturation. This is so because the volume of voids is lower in sample of higher relative density.

4.2 Number of Cycles Required for Initial Liquefaction (N_i)

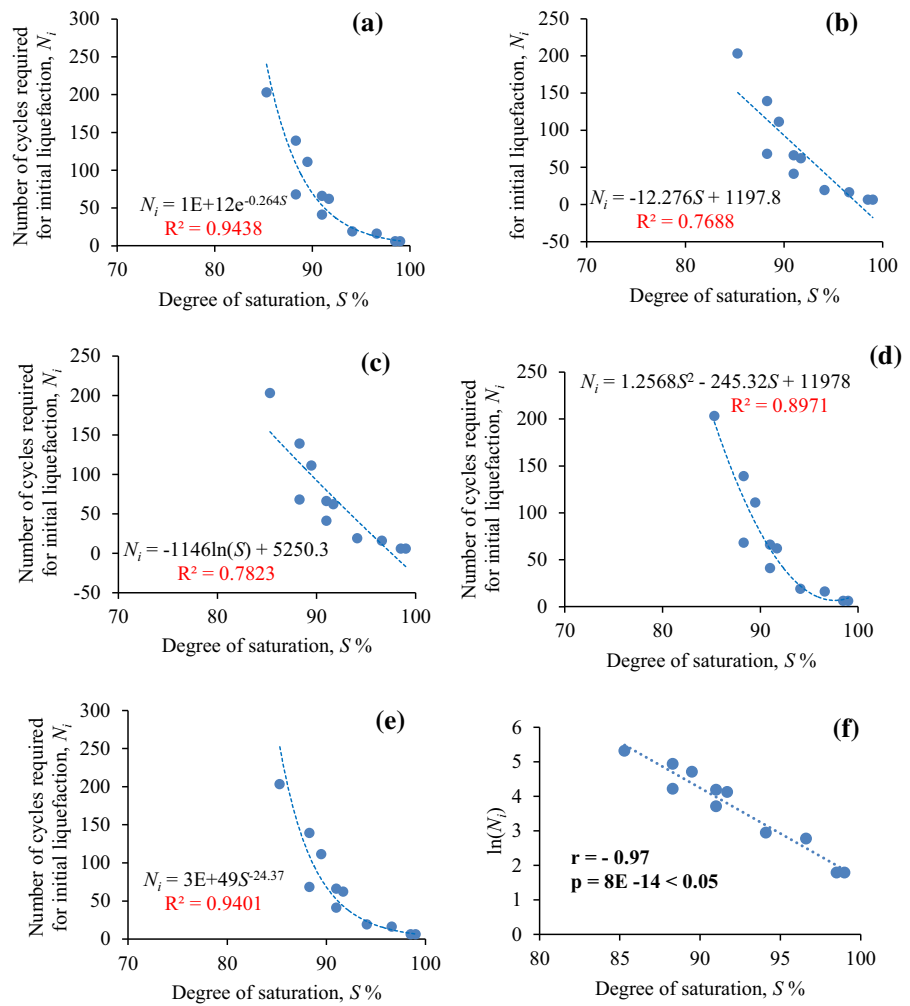
In this section, number of cycles required for initial liquefaction (N_i) of desaturated samples of different degrees of saturation (S) as a function of relative density, initial effective confining pressure and CSR are discussed in detail. It should be noted that in the present study, pore air pressure is assumed to be equal to the pore water pressure. That is, pore water pressure and pore air pressure were not measured separately. This is so because, for the type of sand used in the present study and for the range of degree of saturation considered, matric suction is negligible i.e., around 3–4 kPa (Okamura and Soga, 2006; Unno et al., 2008; Likos and Jaafar, 2013). It should be noted that similar approach was adopted by Okamura and Soga (2006).

Samples with relative density of 30%, 40% and 60% were tested. Tests were conducted at CSR of 0.175, 0.250 and 0.300 and initial effective confining pressure of 50 kPa and 100 kPa. Experimental work was started with sample of D_r 40%, CSR 0.175 and σ'_c 100 kPa. Around 11 tests were conducted for this case and results are plotted in Fig. 5. To understand the trend between N_i and S , different trendlines were fit for this data. The trendlines along with R-squared value and fitting equation are shown in Fig. 5. It is observed that linear and logarithmic fits result into negative number of cycles for S 99 which is absurd from practical point of view. Exponential, power and polynomial trendlines results into positive N_i at all S . However, R-squared value of exponential curve is larger than other two. Therefore, it can be inferred that exponential curve is best possible fit between N_i and S . Thus, N_i increases exponentially with decrease in the degree of saturation (S) of the sample.

4.2.1 On the Exponential Correlation Between N_i and S

It is a well-established fact that regression and correlation are two different things. While former is used to compute numerical value of dependent variable from independent variable, later is used to study if there exists any correlation between two variables. To see if there exists exponential relationship between N_i

Fig. 5 Selection of best fit between N_i and S :
a exponential trendline
b linear trendline
c logarithmic trendline
d polynomial trendline
e power trendline and
f assessing exponential correlation between N_i and S , D_r 40 CSR 0.175, σ'_c 100 kPa



and S , the exponential equation $N_i = 1E12 \times e^{-0.264S}$ was converted into logarithmic one, $\ln N_i = \ln(1E12) - 0.264S$ and correlation coefficient was evaluated for a plot between $\ln N_i$ and S as shown in Fig. 5f. It is observed that the correlation coefficient is -0.97 . This implies that there is very strong exponential correlation between S and N_i . Negative sign implies that as degree of saturation decreases, N_i increases. Once the trend was ascertained, relatively small number of tests were conducted for other cases. From Fig. 6 it can be concluded that N_i increases exponentially with decrease in the degree of saturation (S), irrespective of initial effective confining pressure, relative density and CSR .

Theoretically, as the degree of saturation (S) reduces, the number of cycles required for initial liquefaction (N_i) should increase in such a way that for degree of saturation (S) of 0%, N_i should be infinity. In other words, S versus N_i curve should be an asymptote to the N_i axis. Practically speaking, there would be a certain value of S (other than 0%) for which N_i would be infinitely large. The exponential nature of the S - N_i curves observed in this study is in agreement with theoretical argument and practical consideration. Further, N_i at S 75% is predicted from the respective fitting curve / trend line equations and is given in Table 4 for various combinations of D_r , CSR and σ'_c . From Table 4 it is clear that all three factors *i.e.*,

Fig. 6 Degree of saturation (S) versus number of cycles required for initial liquefaction (N_i)

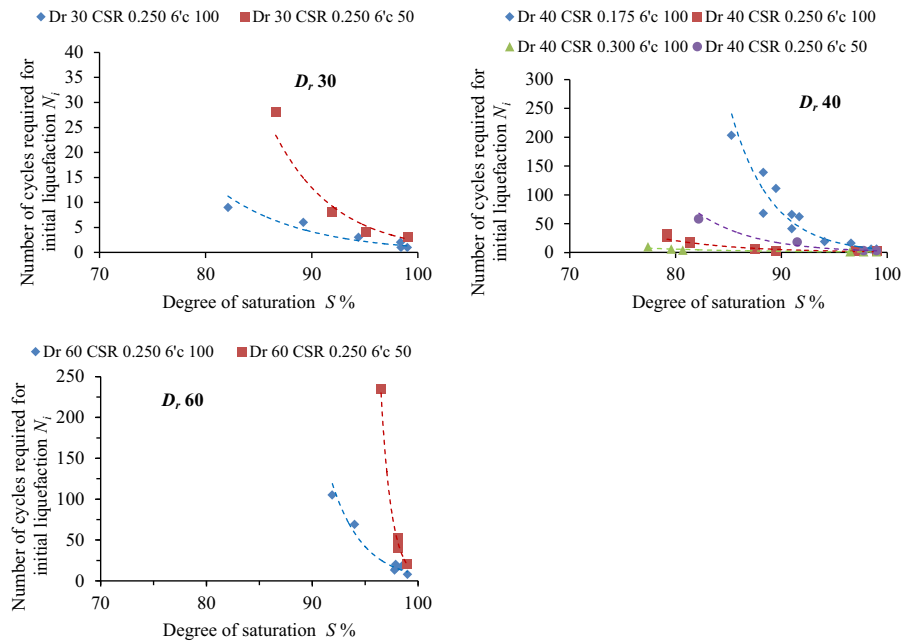


Table 4 Slope M of S — $\text{Log}(N_i)$ curves and predicted N_i at degree of saturation of 75%

Relative density D_r	Initial effective confining pressure σ'_c	CSR	N_i	M
30	100	0.250	28	0.058
	50	0.250	180	0.072
40	100	0.175	2518	0.114
	100	0.250	55	0.060
	100	0.300	10	0.038
	50	0.250	283	0.077
	100	0.250	34,112	0.125
60	100	0.250	34,112	0.125
	50	0.250	4.4×10^{11}	0.447

relative density, CSR and initial effective confining pressure, have significant effect on N_i at S 75%.

4.3 Effect of CSR and Relative Density on N_i

In this section effect of CSR and relative density on N_i is investigated. The variation between CSR and N_i for given S , keeping relative density (40%) and initial effective confining pressure (100 kPa) constant is shown in Fig. 7a. The values of N_i for given S are computed from the exponential equations obtained in Sect. 4.2. Logarithmic scale is used for N_i axis to show all plots effectively. As observed in the figure, as CSR increases, there is reduction in the N_i for given S . The best fit curve with highest R-squared value is found to

be exponential. It should be noted here that being shown on semi-log scale, exponential plot appears to be a straight line. Further, effect of relative density on N_i , keeping CSR (0.250) and initial effective confining pressure (100 kPa) constant is shown in 7b. It is observed that as relative density increases N_i also increases. The best fit curve is found to be exponential.

4.4 Mechanism Behind Increase in N_i on Reduction in S

It is worth noting here that increase in N_i with reduction in S is owing to the compressibility of pore fluid i.e., air–water mixture, and not due to matric suction. This is so because in case of clean sand with

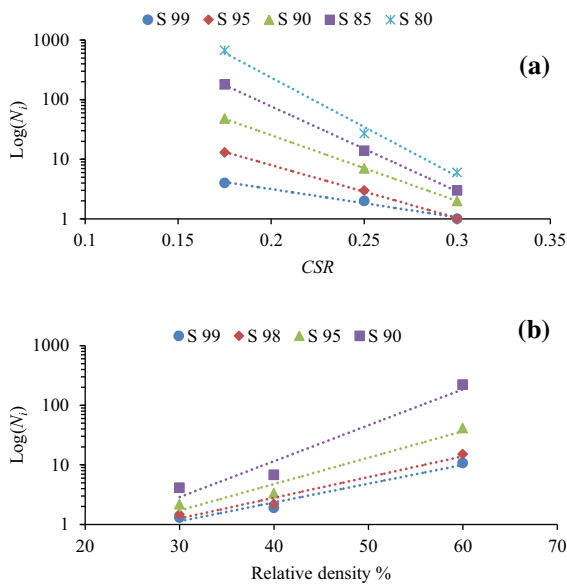


Fig. 7 Effect of CSR and relative density on N_i

degree of saturation in the range of 70% to 99%, matric suction is negligible. It was found by Okamura and Soga (2006) that for a fine clean sand matric suction was at most 4 kPa for S of as low as 70%. Further, Likos and Jaafar (2013) found that for clean river sand with porosity 0.38 and S 60%, matric suction was just 3 kPa. Thus, in such case, increase in N_i is mainly due to increase in compressibility of pore fluid. The mechanism behind significant increase in N_i on desaturation is explained below:

When sample is fully saturated, in present study S 99%, pore fluid comprises of water which is almost incompressible. Owing to incompressibility of water, pore pressure shoots up fast and initial liquefaction occurs in just few cycles. On desaturation, pore fluid is no more just water but air–water mixture. The presence of air makes the pore fluid compressible. In such a case, during loading, the pore fluid may undergo: 1) compression 2) dissolution. Both of these responses are pressure and temperature dependent. For given temperature, higher is the pressure, more is the compression and dissolution. Out of these two responses, latter needs very high pore pressure and it is time dependent as well (Black and Lee 1973; Fredlund and Rahardjio 1993). Total mean pressure applied, during cyclic loading; in the present study is in the range of 41.66 kPa to 126.66 kPa (*i.e.*, absolute pressure in the range of 142.98 kPa to 227.98 kPa).

The pressure to which entrapped air is subjected may be less than or equal to this total pressure. Further, volumetric coefficient of solubility of air into water at this pressure range and at temperature of 25°C, is in the range of 0.0161 to 0.0387. Moreover, coefficient of diffusion for air in water at 25°C is around 2×10^{-9} m²/s. This implies that amount of air dissolved into water during loading might be negligible. Further, compression of the air bubbles is an instantaneous process and happens at relatively low pressure (Black and Lee 1973). Thus, as the loading continues, the degree of saturation of the sample increases due to compression of the pore air. With subsequent loading, a stage may be reached where the air bubbles attain minimum possible size under given load intensity. At this stage, pore fluid act as almost incompressible fluid and further loading of the sample causes rapid increase in the pore pressure resulting into initial liquefaction.

As lower is the initial degree of saturation (S) of desaturated specimen, higher is the compressibility of the pore fluid and more is the number of cycles required to compress the air bubbles to minimum possible size. This increase in compressibility results into significantly high N_i at low S as observed in Fig. 6.

4.5 Slope of S -Log (N_i) curve

Semi-log plots of degree of saturation (S) versus number of cycles required for initial liquefaction (N_i) are shown in Fig. 8. It is observed from this figure that all plots are straight line irrespective of relative density, CSR and initial effective confining pressure. It is worth to note that the combined effect of degree of saturation, relative density, CSR and effective confining pressure is captured by position and slope of these lines. Higher slope implies that the rate of increase in N_i is higher for given relative density, CSR and effective confining pressure. Slope M of all these lines is given in Table 4. It is observed that M has largest value at D_r 60, CSR 0.250, σ'_c 50 kPa and smallest value at D_r 30, CSR 0.25, σ'_c 100 kPa.

5 Cyclic Strength of Desaturated Sand

Cyclic strength, also called as Cyclic Resistance Ratio (CRR), is defined as CSR required to attain specific strain in specific number of uniform loading cycles

Fig. 8 S -Log (N_i) plots

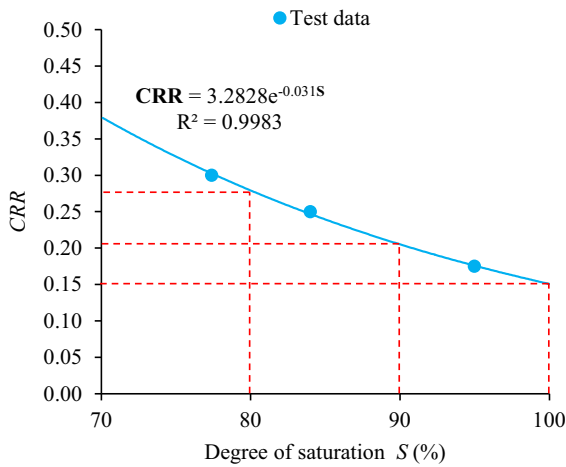
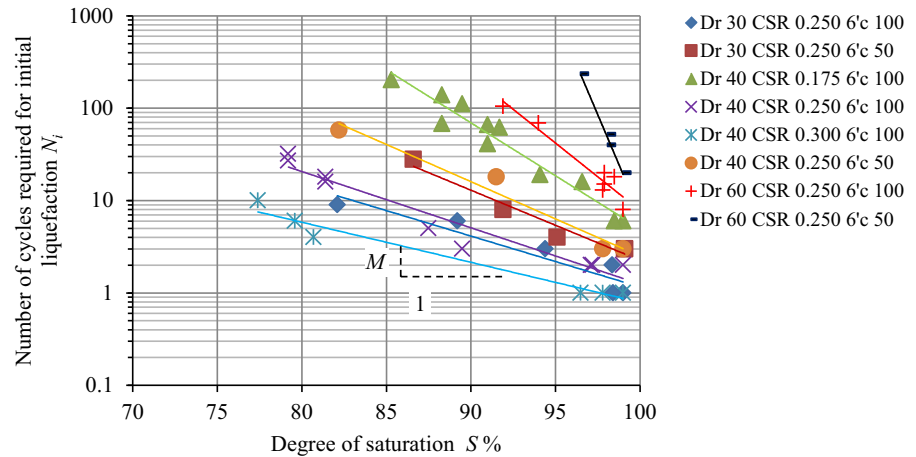


Fig. 9 Cyclic strength of desaturated samples of D_r 40% at σ'_c 100 kPa

(Ishihara 1996; Kramer 1996; Vaid and Sivathayalan 1996; Boominathan and Hari 2002). In this study CRR is defined as the CSR required to attain double amplitude axial strain of 5% in 10 uniform loading cycles. Cyclic strength curve for sample of D_r 40% at effective confining pressure of 100 kPa is shown in Fig. 9. From this figure it is observed that CRR for sample with degree of saturation of 95%, 84% and 77.4% is 0.175, 0.250 and 0.300, respectively. Thus, CRR at degree of saturation of 84% and 77.4% is 1.42 times and 1.71 times, respectively, that of S 95%. Values of CRR at S 100%, 90% and 80%, obtained from extrapolation and interpolation of the exponential fitting curve, are 0.150, 0.205 and 0.280, respectively. Thus, CRR at S of 90% and 80% is 1.37 times and 1.87 times that of S 100%. This implies that in

case of D_r 40% significant increase in liquefaction resistance of sand is obtained when sample is desaturated to S 80%.

For samples of D_r 30% and D_r 60% tests were carried out at initial effective confining pressure of 100 kPa and 50 kPa but at only one CSR i.e., 0.250. The degrees of saturation corresponding to CRR of 0.250 for D_r 30% and D_r 60% are given in Table 5. It is worth to note that in case of D_r 60%, σ'_c 100 kPa, the degree of saturation corresponding to CRR of 0.250 is 98.96%. Further, number of cycles required to reach double amplitude axial strain of 5% is found to be 20 (> 10) in case of S 99, D_r 60 and σ'_c 50 kPa. This implies that cyclic strength of dense sand is significantly high and even small reduction in degree of saturation may result into significant increase in cyclic strength. Similarly, in case of D_r 40%, tests were conducted at initial effective confining pressure of 50 kPa and CSR 0.250. Degree of saturation at CRR 0.250 for D_r 40, σ'_c 50 kPa is found to be 93%.

Cyclic strength, for D_r 40, σ'_c 100 kPa, normalized with respect to cyclic strength at S 100% is shown in Fig. 10. Normalized cyclic strength from some of the previous studies for partly saturated sand is also shown in this figure (Goto and Shamoto, 1987; Yoshimi et al., 1989; Huang et al., 1999; Yasuda et al., 1999; Ishihara et al. 2001a, b). It is observed that in all studies, normalized cyclic strength increases on reduction in degree of saturation. Further, normalized cyclic strength from the present study is close to that from Goto and Shamoto (1987). The difference in the normalized cyclic strength from various studies could be due to: 1) relative density 2) different gradation.

Table 5 CRR and corresponding degree of saturation

Relative density D_r	Initial effective confining pressure σ'_c	S	CRR
30	100	82.77	0.250
	50	91.50	0.250
40	100	95.00	0.175
	100	84.00	0.250
	100	77.40	0.300
	50	93.00	0.250
	100	98.96	0.250
60	100	98.96	0.250
	50	ND ^a	0.250

^aND means cannot be defined

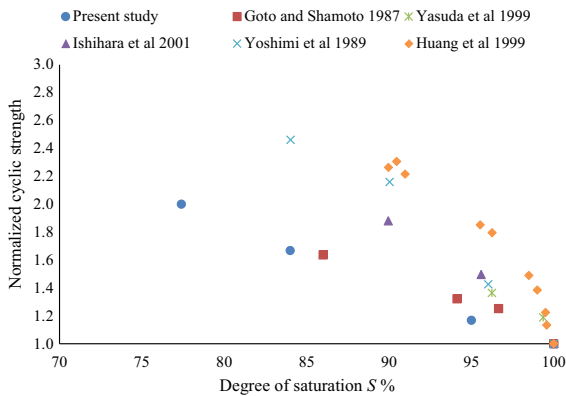


Fig. 10 Comparison of normalized cyclic strength

The tests conducted by Huang et al., (1999) were at relative density of 40% to 70% and σ'_c 98 kPa. Yoshimi et al., (1989) conducted study on sample of D_r 60% and σ'_c 98 kPa. Yasuda et al., (1999) conducted study at D_r 85% and σ'_c 98 kPa. Moreover, all past studies were conducted on partly saturated sand prepared by conventional method.

6 Liquefaction Resistance of Desaturated Sand under Various Earthquake Records from India

In this section, liquefaction resistance of desaturated sand has been assessed against some earthquake records from India. Earthquake records along with peak ground acceleration and magnitude are given in Table 6. As per the study of Iwasaki et al. (1984) liquefaction usually occurs at a depth of 10 m or less. Therefore, in this study soil element at depth of 10 m has been considered. Factor of safety against liquefaction (FS_{liq}) of saturated and desaturated sand of D_r 40% at various degrees of saturation is computed and

given in the Table 6. The procedure adopted to compute FS_{liq} is briefed below:

6.1 Computation of N_{eq}

The equivalent number of uniform stress cycles (N_{eq}) imparted by the given earthquake record is read from an updated m versus N_{eq} chart proposed by Idriss (1997).

6.2 Computation of CSR_{eq} for given earthquake record

The equivalent cyclic shear stress ratio CSR_{eq} for given earthquake record is computed from the following expression (Seed and Idriss 1971).

$$CSR_{eq} = 0.65 \left(\frac{\sigma_v}{\sigma'_v} \right) \left(\frac{a_{max}}{g} \right) r_d \tag{2}$$

where, σ_v and σ'_v are total vertical stress and effective vertical stress at depth z respectively, a_{max} is the peak horizontal acceleration at the ground surface, g is the gravitational acceleration, r_d is the shear stress reduction coefficient at depth z .

For computation of CSR_{eq} , sandy soil used in the present study, with D_r 40%, is assumed to exist at site as well. Water table is assumed to be at ground surface as this represents the worst possible site condition. For computation of σ_v , σ'_v and r_d a soil element at a depth (z) of 10 m is considered. The value of r_d at 10 m depth is 0.92 (Seed and Idriss, 1971). The saturated unit weight of the soil is 19.42 kN/m^3 . The effective vertical pressure at 10 m depth is 96.1 kPa which is very close to initial effective confining pressure of 100 kPa applied in the laboratory study.

Table 6 FS_{liq} of saturated and desaturated sand under various earthquake records

Earthquake	Magnitude (m)	N_{eq}	PGA (g)	CSR_{eq}	FS_{liq} at following degree of saturation					
					100	95	84	77.4	70	65
Bhuj/Kachchh 2001–01-26 03:16:40 UTC	7	10	0.08	0.095	0.87	1.84	2.62	3.15	3.93	4.58
			0.11	0.127	0.65	1.38	1.98	2.37	2.96	3.45
Chamoli 1999–03-28 19:05:11 UTC	6.6	7.5	0.20	0.238	0.39	0.82	1.17	1.40	1.75	2.04
			– 0.36	– 0.430	0.21	0.45	0.65	0.77	0.97	1.13
India-Burma Border 1995–05-06 01:59:07 UTC	6.4	6.6	0.10	0.122	0.79	1.67	2.39	2.87	3.59	4.18
			0.08	0.096	1.00	2.13	3.04	3.64	4.56	5.31
Uttarkashi 1991–10-19 21:23:15 UTC	7	10	– 0.25	– 0.295	0.28	0.59	0.85	1.02	1.27	1.48
			0.25	0.302	0.27	0.58	0.83	0.99	1.24	1.45
		10	– 0.24	– 0.289	0.29	0.61	0.87	1.04	1.30	1.51
India-Burma Border 1988–08-06 00:36:25 UTC	7.2	12	0.31	0.371	0.22	0.47	0.67	0.81	1.01	1.18
			– 0.22	– 0.268	0.29	0.62	0.89	1.06	1.33	1.55
		12	0.15	0.180	0.43	0.92	1.32	1.58	1.97	2.30
		12	– 0.34	– 0.411	0.19	0.40	0.58	0.69	0.87	1.01
			– 0.30	– 0.360	0.22	0.46	0.66	0.79	0.99	1.15

6.3 Conversion of CRR_{lab} to CRR_{field}

It has been suggested by Seed and Idriss (1971) that laboratory cyclic resistance ratio (CRR_{lab}) obtained from cyclic triaxial test should be converted into corresponding field cyclic resistance ratio (CRR_{field}) by using following formula

$$CRR_{field} = C_r(CRR_{lab}) \tag{3}$$

where, C_r is a correction factor. The value of C_r used in the present computations is 0.55 which corresponds to the relative density of 40% (Seed and Idriss, 1971).

It is worth to note that the correction factor C_r recommended by Seed and Idriss (1971) is available only for saturated samples. To date there is no such correction factor available for desaturated samples. In authors’ opinion using same correction factor for desaturated samples may underestimate the cyclic resistance of such samples. Therefore, in the present study, C_r of 0.55 is applied to saturated samples only and for desaturated samples it is assumed to be 1.

6.4 Computation of Factor of Safety Against Liquefaction, FS_{liq}

FS_{liq} is the ratio of CRR_{field} and CSR_{eq} . For FS_{liq} greater than 1 soil is safe against liquefaction. FS_{liq} at different degrees of saturation is given in Table 6. In

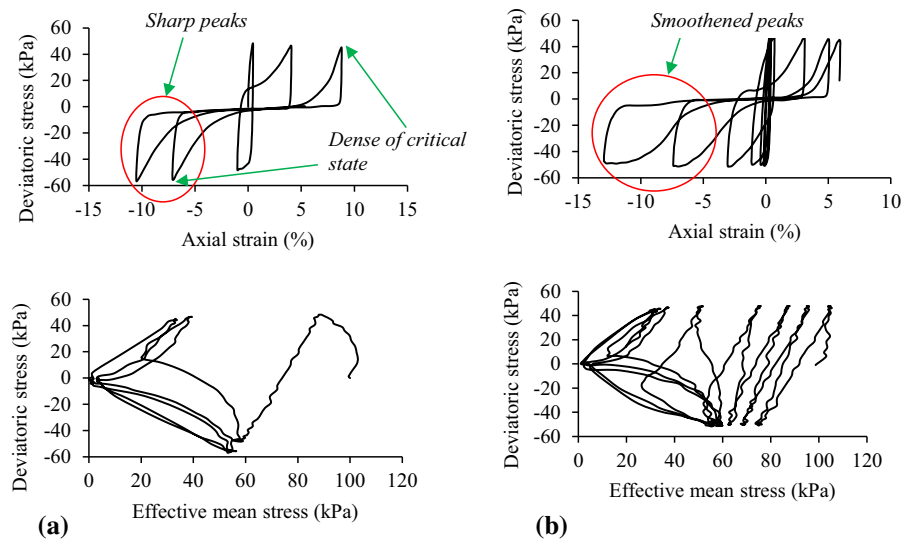
this study, CRR_{lab} corresponds to N 10, which represents the equivalent loading cycles imparted by earthquake of magnitude 7. Therefore, in computation of FS_{liq} , for earthquake of magnitude other than 7, appropriate magnitude scaling factor (MSF) were applied to the CRR_{lab} (Idriss 1999). The MSF applied to earthquake of magnitude 6.4, 6.6 and 7.2 is 1.17, 1.11 and 0.95, respectively.

Further, CRR_{lab} for S 100%, 70% and 65% are obtained by extrapolation from the cyclic strength curve for D_r 40%. It is observed from Table 6 that at S 70% FS_{liq} is greater than 1 for earthquake records with peak ground acceleration up to 0.3 g. Further, at S 65% FS_{liq} is greater than 1 for earthquake records with peak ground acceleration as high as 0.36 g. It can be concluded from this discussion that desaturation up to S 70% is adequate to prevent liquefaction under moderate to strong earthquakes.

7 Failure Modes

From present study it is observed that desaturation not only affects the liquefaction resistance but also patterns of stress strain curve and effective stress path. Depending on S , CSR , D_r and σ'_c , three distinct stress strain curves are observed in this study. These

Fig. 11 Cyclic mobility observed at σ'_c 100 kPa, CSR 0.25 for D_r 30%: **a** S 99% **b** S 89.2%



are herein called as failure modes. A detailed discussion on failure modes is held in the following section.

7.1 Cyclic Mobility

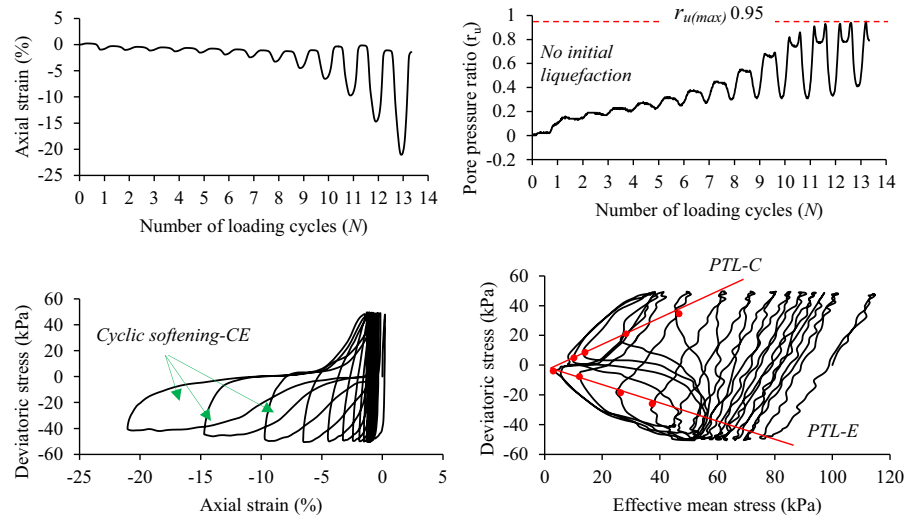
Cyclic response of saturated (S 99%) and desaturated samples (S 89.2%) of relative density of 30% at initial effective confining pressure of 100 kPa and CSR 0.25 is shown in Fig. 11. It is clear from this figure that both saturated and desaturated samples undergo typical cyclic mobility failure. In this type of failure, sample reaches a dense of critical state during both compression and extension stage of loading; which is indicated by the peaks in stress strain curve as seen in Fig. 11. It should be noted here that at degree of saturation of 89.2% smoothed peaks on extension side of stress strain curve are observed.

Smoothed peaks indicate that, in this case, sample reaches dense of critical state at slower rate than their saturated counterparts thereby undergoing relatively large axial straining. This inference can be justified from the stress strain curve of this sample shown in Fig. 11. From Fig. 11 it is observed that saturated sample of D_r 30% undergoes axial straining from -7 to -10.5% i.e., net axial straining of 3.5%, over last two cycles whereas sample with S 89.2% undergoes relatively large straining from -7 to -13% i.e., net axial straining of 5% > 3.5%, over last two cycles. Similar response was observed for samples of relative density of 40% and 60% but for brevity not shown.

7.2 Cyclic Softening-CE

In this study it is found that samples at low degree of saturation mostly below 75%, if fails depending on CSR , D_r and σ'_c , undergoes failure different from cyclic mobility. Failure of a sample of degree of saturation 74% and relative density of 30%, at initial effective confining pressure (σ'_c) of 100 kPa and CSR 0.25, is shown in Fig. 12. The stress strain curve observed in this case is completely different from stress strain curve of cyclic mobility. Sample undergoes deformation on extension side as opposed to relatively symmetric deformation observed in cyclic mobility. The maximum pore pressure ratio attained during loading is 0.95. Though pore pressure ratio is well below 1, sample undergoes large deformation due to cyclic softening. The double amplitude axial strain (DA), in this case, is as high as 21.26%. From the effective stress path it is clear that sample undergoes phase transformation during both compression and extension stage of loading, over last few cycles. This phase transformation has been shown by two lines, PTL-C and PTL-E drawn on effective stress path, where, PTL-C stands for phase transformation line during compression and PTL-E stands for phase transformation line during extension. In the present study, this type of failure is entitled as cyclic softening-CE. It is worth to note that in this case sample did not attain r_u of 1. However, it developed significantly high pore pressure, r_u 0.95, which reduced the stiffness of sample which eventually

Fig. 12 Cyclic softening-CE of a sample at low degree of saturation (S 74%) of D_r 30% at σ'_c 100 kPa, CSR 0.25



resulted into failure. Similar, response was also observed for samples at low degree of saturation of relative density of 40% and σ'_c 100 kPa.

7.3 Cyclic Softening-E

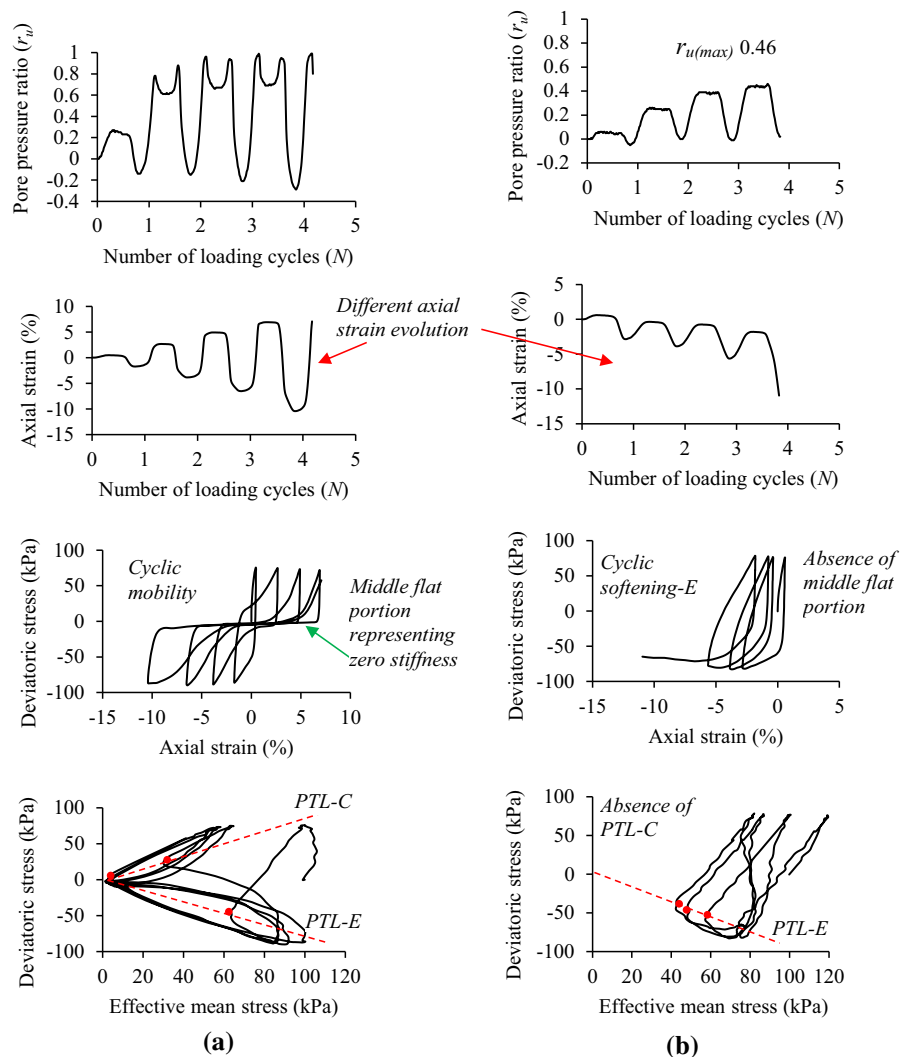
Few tests were conducted on samples of relative density of 60% at CSR of 0.4 and initial effective confining pressure (σ'_c) of 100 kPa. The response of saturated sample (S 99%) and sample with S 83.6% is shown in Fig. 13. From the stress strain curve and pore pressure ratio evolution plot it is clear that saturated sample undergoes cyclic mobility failure and develops negative pore pressure during extension stage of the loading. It should be noted that saturated sample of same relative density subjected to CSR of 0.25 and initial effective confining pressure (σ'_c) of 100 kPa showed reduction in the pore pressure during extension stage of loading but it never attained negative pore pressure value. This finding implies that for a saturated sample, dilative tendency is more intense at higher CSR , during extension stage of loading, than at lower CSR .

It is observed that in spite of having very low degree of saturation, sample with S 83.6% underwent significantly large axial deformation on extension side due to cyclic softening as seen in Fig. 13b. From the effective stress path and pore pressure ratio plot it is clear that this sample undergoes phase transformation during extension stage of loading only. Therefore, in present study it is named as cyclic softening-E.

Further, the maximum pore pressure ratio attained in this case was just 0.46. The large straining of the sample observed at this low pore pressure ratio and CSR 0.4, has been explained as follows: When sample is saturated and it tries to dilate, during compression or extension stage of loading, surface tension develops in the pore water which in turn reduces the pore pressure significantly as seen in Fig. 13a. This reduction in the pore water pressure increases the effective confining pressure which in turn increases the stiffness of the sample. This increase in the stiffness prevents large deformation of the sample during corresponding stage of loading.

In case of sample with S 83.6%, significant amount of air is present in the voids along with water. The presence of large amount of air makes pore fluid highly compressible. This compressibility prevents generation of high pore water pressure during compression stage of loading as shown in Fig. 13b. As pore pressure is low, stiffness of the sample remains high compared to its nearly saturated counterpart, during this stage of loading. Therefore, sample undergoes very small deformation on compression side. As deformation is very small, dilative tendency does not develop during this stage of loading. The absence of dilative tendency is supported by absence of phase transformation line on compression side (PTL-C) in Fig. 13b. When sample is subjected to extension stage of loading, sample tries to dilate. But due to presence of air, surface tension in pore water does not develop to the extent it got developed in its

Fig. 13 Cyclic mobility and cyclic softening observed at $CSR\ 0.4$ for $D_r\ 60\%$ at $\sigma'_c\ 100\ \text{kPa}$: **a** Cyclic mobility, $S\ 99\%$ **b** Cyclic softening-E, $S\ 83.6\%$



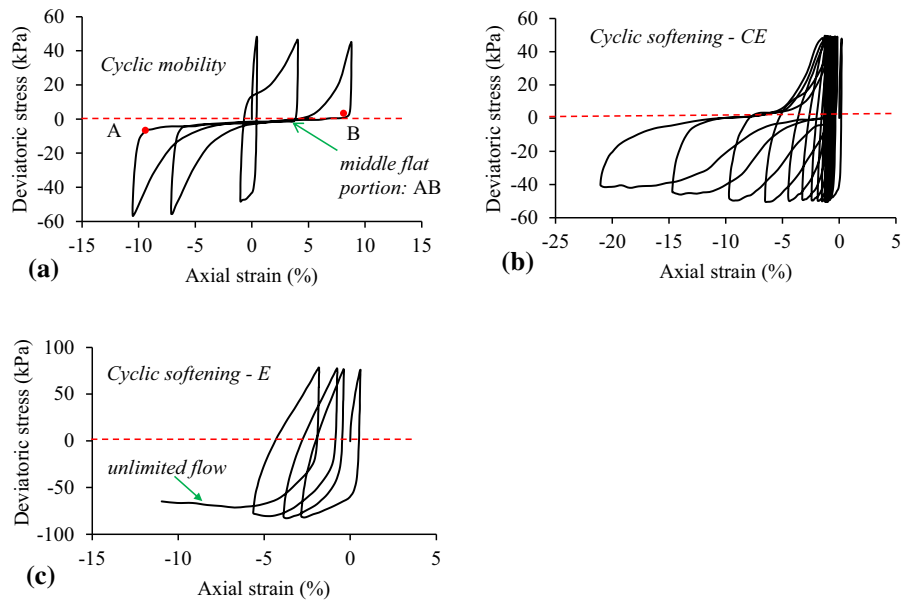
saturated counterpart. Therefore, during this stage of loading pore water pressure reduces but not to the extent observed in saturated sample. It means that stiffness of the sample remains low during this stage of loading which in turn results into large axial deformation on extension side. Further, the alternate dilative and contractive tendency observed during extension stage of loading gives rise to a phase transformation line (PTL-E) as shown in Fig. 13b.

Typical stress strain curves observed during various failure modes are summarized in Fig. 14. It should be noted that middle flat portion AB at zero deviatoric stress observed in cyclic mobility is absent in Cyclic softening-CE and Cyclic softening-E.

8 Pore Pressure Model for Desaturated Sand

In this study, an attempt has been made to propose pore pressure model for desaturated sand. In authors knowledge, pore pressure model for desaturated sand is yet to be developed. However, there are quite a few pore pressure models for saturated sand (Booker et al. 1976; Seed and Lysmer 1976; Ishibashi et al. 1977; Ishibashi et al. 1982; Konstadinou and Georgiannou 2014). A comprehensive model that takes care of stress history, loading cycles, shear stress amplitude, density and effective confining stress is one developed by Konstadinou and Georgiannou (2014). Based on their extensive study, they proposed an equation, along with some constants, to predict the pore pressure

Fig. 14 Comparison of typical stress–strain curves for different failure modes: depends on S , CSR , D_r and σ'_c



build up. However, this model does not incorporate effect of partial saturation/desaturation on pore pressure build up. In present study, this model has been modified to take care of desaturation.

The equation proposed by Konstadinou and Georgiannou (2014) is given below:

$$\begin{aligned}
 (\Delta r_u)_N = & (1 - (r_u)_{N-1}) \cdot \left(\frac{\tau_{\theta z}}{p'_{N-1}} \right)^n \cdot f(e)^d \cdot \left(\frac{p'_i}{p_a} \right)^c \\
 & \cdot \left[\frac{C_1}{N C_2 + C_3 \cdot N} + C_4 \cdot C_1 \right]
 \end{aligned}
 \tag{4}$$

where, $(\Delta r_u)_N$ is the incremental residual pore pressure ratio at the end of N^{th} loading cycle, $(r_u)_{N-1}$ is the residual pore pressure ratio at the end of $(N-1)^{\text{th}}$ loading cycles, $\tau_{\theta z}$ is torsional shear stress, p'_{N-1} is the effective mean stress at the end of $(N-1)^{\text{th}}$ cycle, p'_i is the initial effective mean stress at the end consolidation, p_a is the atmospheric pressure, $f(e) = (2.17 - e^2) / (1 + e)$, e is the initial void ratio of the sample, $n = 2.4$ for $(\tau_{\theta z} / p'_{N-1}) \leq 0.6 (\tau_{\theta z} / p')_{PTL/IL}$ and $n = 6.8$ for $(\tau_{\theta z} / p'_{N-1}) > 0.6 (\tau_{\theta z} / p')_{PTL/IL}$; $(\tau_{\theta z} / p')_{PTL/IL}$ is the ratio corresponding to phase transformation line or instability line. $d = 0.632 \ln(N) - 3.087$; $c = -0.034 N + 0.68$ for $N < 20$ and $c = 0$ for $N \geq 20$; C_2 , C_3 and C_4 are sand independent

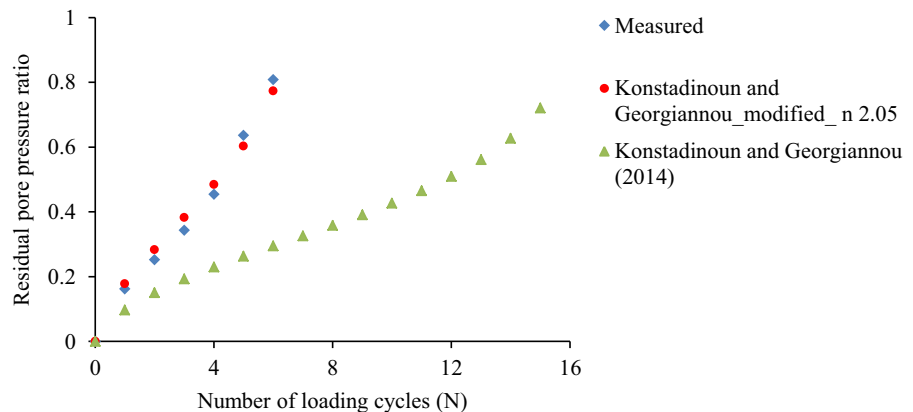
constants having values 1.8, 2.0 and 0.015 respectively. C_1 is the sand dependent constant. For more details readers are referred to Konstadinou and Georgiannou (2014).

In the present study, Konstadinou and Georgiannou (2014) model has been modified to incorporate desaturation effect. In their study, CSR was in the range of 0.109 and 0.25; and initial mean effective stress was in the range of 100 kPa and 320 kPa. In the present study, this equation has been modified for CSR of 0.175 and 0.25 for samples of D_r 40% at σ'_c 100 kPa. After careful study of Konstadinou and Georgiannou (2014) model it was realized that this model needs to modify for two effects: 1) modification to incorporate CSR effect 2) modification to incorporate desaturation effect, as explained below.

8.1 Modification for CSR effect:

To begin with, pore pressure measured for S 99%, CSR 0.175 and σ'_c 100 kPa is compared with that predicted by Konstadinou and Georgiannou (2014) model as shown in Fig. 15. Value of C_1 was chosen to be 52. This is so because, this value corresponds to mean particle size (D_{50}) of 0.29 mm from Konstadinou and Georgiannou study, which is very close to mean particle size (D_{50}) of 0.27 mm from the present study. Other constants were taken as it is, suggested by Konstadinou and Georgiannou. From Fig. 15 it is

Fig. 15 Residual pore pressure evolution for S 99%, D_r 40%, CSR 0.175 and σ'_c 100 kPa



observed that number of cycles required to reach initial liquefaction are 15 in case of Konstadinou and Georgiannou model whereas experimentally measured cycles are just 6. Thus, number of cycles predicted by Konstadinou and Georgiannou model is 2.5 times number of the observed cycles. On careful study of Konstadinou and Georgiannou model, it was realized that main cause of this discrepancy is the way CSR is defined in Konstadinou and Georgiannou study and present study. Konstadinou and Georgiannou conducted tests on hollow cylinder torsional shear tests and present study tests were conducted on cyclic triaxial test. This results into different definitions of CSR . In torsional shear test, shear stress applied directly on the horizontal plane is considered in definition of CSR whereas in cyclic shear test shear stress induced on the 45° plane is considered for CSR . It should be noted that in Eq. (4), n parameter takes care of CSR . Therefore, in present study this parameter was altered so that measured and predicted pore pressure match well. From several trials it was found that when n was chosen to be 2.05, there is excellent agreement between measured and predicted pore pressure as seen in Fig. 15.

8.2 Modification for Desaturation Effect

For given relative density, desaturated sample takes more N_i than its saturated counterpart. Similarly, saturated sample of higher relative density takes more N_i than saturated sample at lower relative density. Thus, desaturation of given sample is analogous to increase in its relative density. In Konstadinou and Georgiannou (2014) model, void ratio function $f(e)$,

raised to exponent d , takes care of the density effect on evolution of pore pressure. In present study, the exponent d has been modified to take care of desaturation; in such a way that there is good agreement between measured and predicted pore pressure. While doing so, the constant term 3.87 of $d = 0.632 \ln(N) - 3.87$, has been modified with respect to degree of saturation. In present study, d is defined as $d = 0.632 \ln(N) - d''$, where d'' is the constant which is function of degree of saturation. In addition to this, n parameter was also required to change from 2.05 to 1 after reaching critical stress ratio. Critical stress ratio is the ratio (τ/p'_{N-1}) at critical cycle, $N_{critical}$, where, τ is the amplitude of cyclic shear stress which is half of cyclic deviatoric stress. $N_{critical}$ is the cycle at which residual pore pressure changes from Stage 2 to Stage 3 as shown in Fig. 16. In Stage 1 pore pressure increases with decreasing rate, in Stage 2 pore pressure increases with constant rate and in Stage 3 pore pressure increases with increasing rate. To understand Stage 1–3, plot of incremental residual pore pressure ratio evolution shown in Fig. 16 should be referred to.

In Fig. 17, pore pressure evolution for S 91%, D_r 40%, CSR 0.175 and σ'_c 100 kPa is shown for various conditions. Here, d'' is 9.8. Predicted pore pressure is shown for two cases: Case 1) n 2.05 throughout loading cycles and Case 2) n 2.05 up to critical stress ratio and there onwards n 1.0. Also shown is the measured pore pressure evolution. It is clear that when n 2.05 is used throughout, predicted pore pressure evolution fails to capture rise in pore pressure in Stage 3. On the other hand, when n is changed to 1 on reaching $N_{critical}$, rise in pore pressure in Stage 3 is captured very well. Moreover, there is excellent

Fig. 16 Different Stages in evolution of residual pore pressure ratio (S 91%, CSR 0.175, D_r 40% and σ'_c 100 kPa)

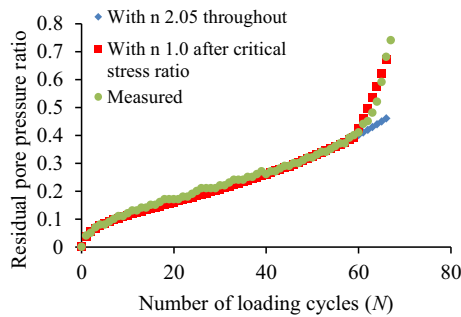
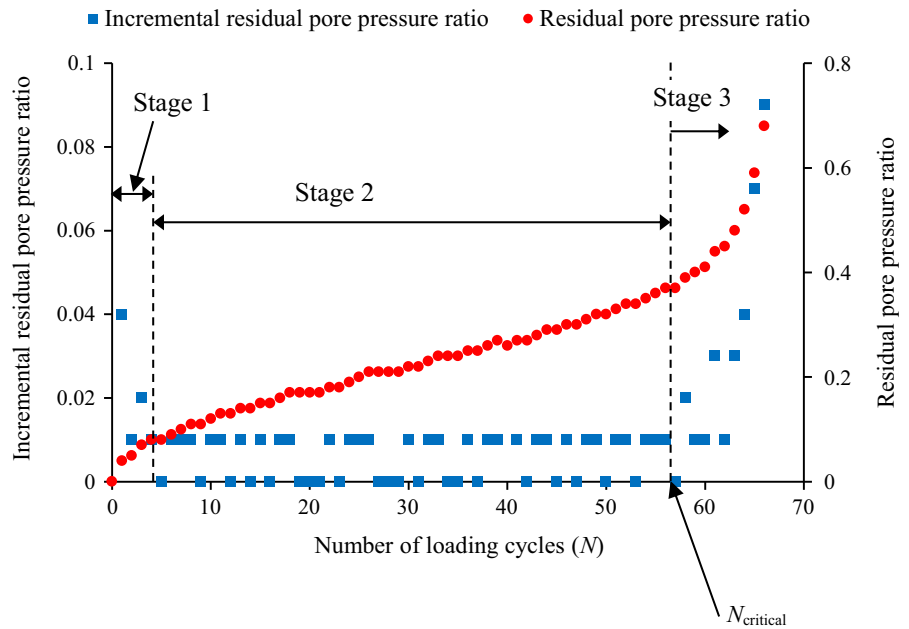
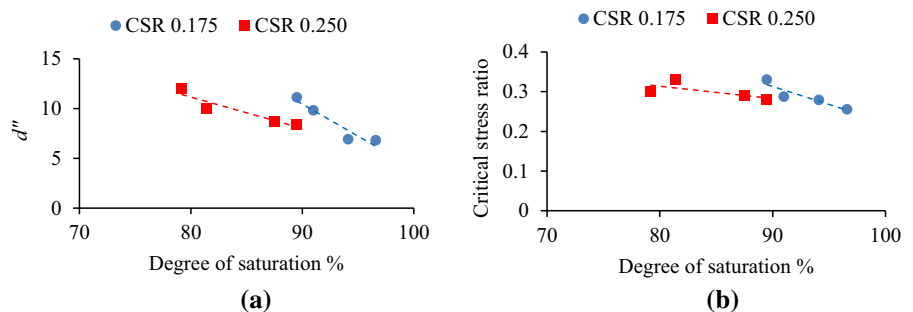


Fig. 17 Effect of n on evolution of pore pressure ratio, S 91%, CSR 0.175, D_r 40% and σ'_c 100 kPa

agreement between measured and predicted pore pressure (with Case 2) as seen in Fig. 17.

Variation of d'' and critical stress ratio with degree of saturation is shown in Fig. 18. It is observed that both parameters increase with decrease in S . In case of

Fig. 18 Variation of d'' and critical stress ratio with degree of saturation



CSR 0.175, critical stress ratio spans from 0.255 to 0.33 whereas in case of CSR 0.250 it spans from 0.28 to 0.33. The average critical stress ratio is found to be 0.29 and 0.30 for CSR 0.175 and 0.250, respectively.

Moreover, comparison between predicted and measured pore pressure for desaturated samples of various degrees of saturation is shown in Fig. 19. Predicted pore pressure is computed after incorporating above mentioned modifications to Konstadinou and Georgiannou (2014) model. It is observed that there is very well agreement between predicted and measured pore pressure. However, authors feel that further study is required in this direction, to propose more generalized pore pressure model for desaturated sand.

Fig. 19 Comparison of measured and predicted residual pore pressure ratio

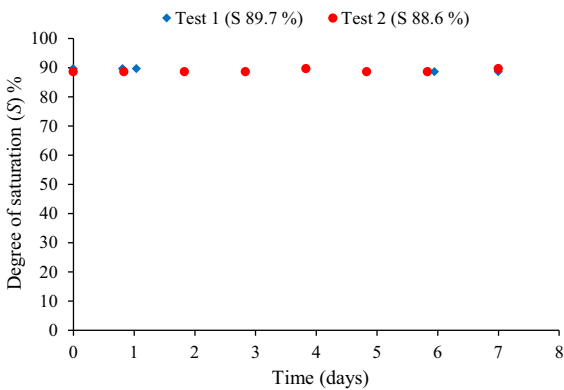
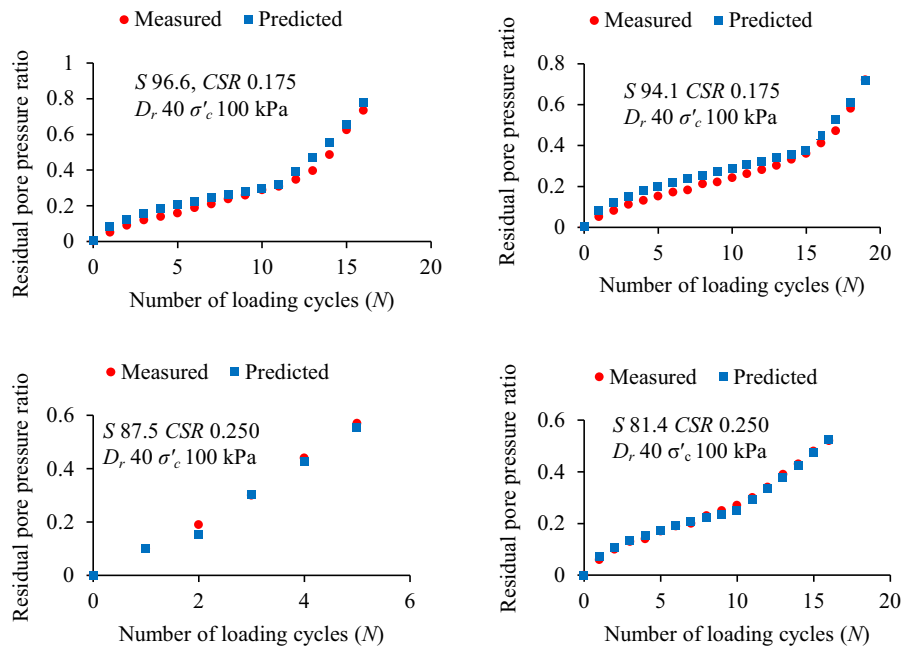


Fig. 20 Variation in the degree of saturation (S) of the desaturated sample with time

9 Longevity of Entrapped Air

Longevity test had been conducted to assess the change in the degree of saturation of the desaturated sample over the period of 7 days. In this test, sample was first desaturated and B parameter was measured at different intervals of time, from which degree of saturation was computed. Two tests were conducted on desaturated samples with initial degree of saturation of 89.7% and 88.6%, respectively. It was observed that the change in the degree of saturation

of both samples was just 1% at the end of 7 days, as shown in Fig. 20.

It was found by other researchers that the entrapped air bubbles could survive as long as 26 years (Okamura et al. 2006). They found a degree of saturation as high as 92% even at the end of 26 years at a site which in past had been desaturated during construction of Sand Compaction Piles (SCP). It was further claimed by them that if the degree of saturation on desaturation is below 90%, desaturation condition can survive for a long time.

10 Conclusion

In this study, response of desaturated clean sand subjected to cyclic loading has been investigated in depth with large number of tests. Various issues such as cyclic strength, modes of failure, pore pressure evolution, number of cycles required for initial liquefaction (N_i) etc. have been explored. In addition to this, performance of desaturated sand under some earthquake records from India has also been assessed. Major findings from the present study are summarized below:

- a) Number of cycles required for initial liquefaction (N_i) increased exponentially with decrease in the degree of saturation, irrespective of the initial

effective confining pressure, relative density and *CSR*. It is observed that for given *S*, keeping relative density (40%) and initial effective confining pressure (100 kPa) constant, N_i decreased exponentially with increase in *CSR*. Further, for given *S*, keeping *CSR* (0.250) and initial effective confining pressure (100 kPa) constant, N_i increased exponentially with increase in relative density b) There is significant increase in the cyclic strength of the sand on desaturation. Cyclic strength of the desaturated sample of relative density of 40% at degree of saturation 80% is found to be twice that of saturated sample. c) Desaturation up to degree of saturation of 70% is adequate to prevent liquefaction of clean sand under moderate to strong earthquakes having peak ground acceleration as high as 0.30 g. d) Samples with high degree of saturation underwent cyclic mobility failure whereas sample at low degree of saturation underwent either cyclic softening-CE or cyclic softening-E. e) Evolution of pore pressure in desaturated sand can be predicted by modifying Konstadinou and Georgiannou (2014) model for *CSR* effect and desaturation effect. f) It has been found that there is negligible change in the degree of saturation of the desaturated sample at the end of 7 days. This implies that the entrapped air bubbles in the sample do not dissolve into the pore water over the period of time.

Declarations

Conflict of interest The authors have no conflicts of interest to declare.

References

- ASTM:D5311/D5311M-13 (2013) *Standard Test Method for Load Controlled Cyclic Triaxial Strength of Soil*. doi: <https://doi.org/10.1520/D5311>.
- Black D, Lee K (1973) Saturating laboratory samples by back pressure. *Journal of Soil Mechanics & Foundations Div* 99(SM1):75–95
- Booker, J. R., Rahman, M. S. and Seed, H. B. (1976) *GAD-FLEA: A computer program for the analysis of pore pressure generation and dissipation during cyclic or earthquake loading Berkeley: Earthquake Engineering Center, University of California*.
- Boominathan A, Hari S (2002) Liquefaction strength of fly ash reinforced with randomly distributed fibers. *Soil Dyn Earthq Eng* 22:1027–1033
- Celestino V, Kenneth H (2012) Seismic measurements in sand specimens with varying degrees of saturation using piezoelectric transducers. *Can Geotech J* 685(152):671–685. <https://doi.org/10.1139/T2012-033>
- Eseller-bayat E, Yegian MK, Alshawabkeh A (2013) Liquefaction response of partially saturated Sands. i: experimental results. *J Geotechnical Geoenvironmental Eng* 139(6):863–871. [https://doi.org/10.1061/\(ASCE\)GT.1943-5606.0000815](https://doi.org/10.1061/(ASCE)GT.1943-5606.0000815)
- Fredlund DG, Rahardjo H (1993) *Soil mechanics for unsaturated soils*, JOHN WILEY & SONS. JOHN WILEY & SONS, INC., INC. [https://doi.org/10.1016/0267-7261\(93\)90011-F](https://doi.org/10.1016/0267-7261(93)90011-F)
- Goto, S. and Shamoto, Y. (1987) 'Estimation method for the liquefaction strength of unsaturated sandy soil (part 2)', in *37th Jpn. Nat. Conf. Geotech. Engrg.*
- He J, Chu J (2012) (2014) 'Undrained Responses of Microbially Desaturated Sand under Monotonic Loading.' *Journal of Geotechnical and Geoenvironmental Engineering* 140:04014003. [https://doi.org/10.1061/\(ASCE\)GT.1943-5606.0001082](https://doi.org/10.1061/(ASCE)GT.1943-5606.0001082)
- He J, Chu J, Ivanov V (2013) Mitigation of liquefaction of saturated sand using biogas. *Géotechnique* 63(4):267–275. <https://doi.org/10.1680/geot.SIP13.P.004>
- Huang, Y., Tsuchiya, H. and Ishihara, K. (1999) 'Estimation of partial saturation effect on liquefaction resistance of sand using P-wave velocity.', in *Proc. JGS Symp (Vol. 113)*, pp. 431–434.
- Idriss, I. M. (1997) 'Evaluation of liquefaction potential and consequences: Historical perspective and updated procedure', in *Presentation notes, 3rd Short Course on Evaluation and Mitigation of Earthquake Induced Liquefaction Hazards*. San Francisco.
- Idriss, I. M. (1999) 'An update to the Seed-Idriss simplified procedure for evaluating liquefaction potential', in *TRB Workshop on New Approaches to Liquefaction Publ. n. FHWA-RD-99-165, Federal Highway Administration*.
- Idriss, I. M. and Boulanger, R. . (2008) *Soil liquefaction during earthquakes*. EERI.
- Ishibashi I, Sherif MA, Tsuchiya C (1977) Pore-pressure rise mechanism and soil liquefaction. *Soils Found* 17(2):17–27
- Ishibashi, I., Sherif, M. A. and Cheng, W. L. (1982) 'The effects of soil parameters on pore-pressure-rise and liquefaction prediction.', *Soils and Foundations*, 22(1), pp. 39–48.
- Ishihara, K. (1996) *Soil Behaviour in Earthquake Geotechnics*. Oxford Science Publications.
- Ishihara, K *et al.* (2001) 'Keynote Lecture: Recent Studies on Liquefaction Resistance of Sand-Effect of Saturation', in *Fourth International Conference on Recent Advances in Geotechnical Earthquake Engineering and Soil Dynamics*.
- Ishihara, K. *et al.* (2001) 'Recent studies on liquefaction resistance of sand-effect of saturation', in *4th International Conference on Recent Advances in Geotechnical Earthquake Engineering and Soil Dynamics*.
- Ishihara, M., Okamura, M. and Oshita, T. (2003) 'Desaturating sand deposit by air injection for reducing liquefaction potential', *Pacific Conference on Earthquake Engineering.*, (89).
- Iwasaki T, Arakawa T, Tokida KI (1984) Simplified procedures for assessing soil liquefaction during earthquakes. *Int J Soil Dynamics Earthquake Eng* 3(1):49–58
- Kato K, Nagao K (2020) Numerical evaluation of liquefaction resistance for desaturated sands. *J Geotechnical*

- Geoenvironmental Eng 146(6):04020037. [https://doi.org/10.1061/\(asce\)gt.1943-5606.0002234](https://doi.org/10.1061/(asce)gt.1943-5606.0002234)
- Kokusho T (2000) Correlation of pore-pressure B- value with P-wave velocity and poisson's ratio for imperfectly saturated sand or gravel. *Soils Found* 40(4):95–102. <https://doi.org/10.1248/cpb.37.3229>
- Konstadinou M, Georgiannou VN (2014) Prediction of pore water pressure generation leading to liquefaction under torsional cyclic loading. *Soils and Foundations*. <https://doi.org/10.1016/j.sandf.2014.09.010>
- Kramer, S. L. (1996) *Geotechnical Earthquake Engineering*. PEARSON.
- Lade, P. V (2016) *Triaxial Testing of Soils*. First edit. John Wiley & Sons, Ltd.
- Likos, W. J. and Jaafar, R. (2013) 'Pore-Scale Model for Water Retention and Fluid Partitioning of Partially Saturated Granular Soil' doi: [https://doi.org/10.1061/\(ASCE\)GT.1943-5606.0000811](https://doi.org/10.1061/(ASCE)GT.1943-5606.0000811).
- Marasini NP, Okamura M (2015a) Air injection to mitigate liquefaction under light structures. *Int J Phys Modelling Geotechnics* 15(3):129–140. <https://doi.org/10.1680/jphmg.14.00005>
- Marasini NP, Okamura M (2015b) Numerical simulation of centrifuge tests to evaluate the performance of desaturation by air injection on liquefiable foundation soil of light structures. *Soils and Foundations Elsevier* 55(6):1388–1399. <https://doi.org/10.1016/j.sandf.2015.10.005>
- Okamura M, Soga Y (2006) Effects of pore fluid compressibility on liquefaction resistance of partially saturated sand. *Soils Foundations Japanese Geotechnical Society* 46(5):695–700. <https://doi.org/10.3208/sandf.46.695>
- Okamura M, Ishihara M, Tamura K (2006) Degree of saturation and liquefaction resistances of sand improved with sand compaction pile. *J Geotechnical Geoenviron Eng* 132(2):258–264. [https://doi.org/10.1061/\(ASCE\)1090-0241\(2006\)132:2\(258\)](https://doi.org/10.1061/(ASCE)1090-0241(2006)132:2(258))
- Okamura M et al (2011) In-situ desaturation test by air injection and its evaluation through field monitoring and multiphase flow simulation. *J Geotechnical Geoenviron Eng* 137(7):643–652. [https://doi.org/10.1061/\(ASCE\)GT.1943-5606.0000483](https://doi.org/10.1061/(ASCE)GT.1943-5606.0000483)
- Pietruszczak S, Pande GN, Oulapour M (2003) A hypothesis for mitigation of risk of liquefaction. *Géotechnique* 53(9):833–838. <https://doi.org/10.1680/geot.2003.53.9.833>
- Rad NS, Wayne Clough G (1984) New procedure for saturating sand specimens. *J Geotechnical Geoenviron Eng* 110(9):1205–1218. [https://doi.org/10.1061/\(ASCE\)0733-9410\(1984\)110:9\(1205\)](https://doi.org/10.1061/(ASCE)0733-9410(1984)110:9(1205))
- Rees, S. (no date) *What is Triaxial Testing? Part one: Introduction to Triaxial Testing GDS*. Accessed Januray 2017. Available at: www.gdsinstruments.com.
- Seed HB, Idriss IM (1971) Simplified procedure for evaluating soil liquefaction potential. *J Soil Mech Foundations Division* 97(9):1249–1273
- Seed, H. B., P., M. P. and Lysmer, J. (1976) 'Pore-water pressure changes during soil liquefaction', *Journal of Geotechnical and Geoenvironmental Engineering* 102(Proc. Paper# 12074).
- Sherif MA, Tsuchiya C, Ishibashi I (1977) Saturation effects on initial soil liquefaction. *J Geotech Eng Div* 103(8):914–917
- Skempton AW (1954) The pore-pressure coefficients A and B. *Géotechnique* 4(4):143–147. <https://doi.org/10.1680/geot.1954.4.4.143>
- Sze HY, Yang J (2014) Failure Modes of Sand in Undrained Cyclic Loading: Impact of Sample Preparation. *Geotech Geoenviron Eng*. [https://doi.org/10.1061/\(ASCE\)GT.1943-5606.0000971](https://doi.org/10.1061/(ASCE)GT.1943-5606.0000971)
- Takemura, J. et al. (2009) 'Centrifuge model tests on soil desaturation as a liquefaction countermeasure', *Proceedings of the 17th International Conference on Soil Mechanics and Geotechnical Engineering: The Academia and Practice of Geotechnical Engineering*, doi: <https://doi.org/10.3233/978-1-60750-031-5-502>.
- Unno T et al (2008) Liquefaction of unsaturated sand considering the pore air pressure and volume compressibility of the soil particle skeleton. *Soils Found* 48(1):87–99. <https://doi.org/10.3208/sandf.48.87>
- Vaid YP, Sivathayalan S (1996) Static and cyclic liquefaction potential of Fraser Delta sand in simple shear and triaxial tests. *Can Geotech J* 33(2):281–289
- Xin L et al (2016) Small-strain shear modulus of volcanic granular soil: An experimentation investigation. *Soil Dyn Earthq Eng* 86:15–24
- Yang J, Savidis S, Roemer M (2004) Evaluating liquefaction strength of partially saturated sand. *J Geotech Eng Division* 130(9):975–979. [https://doi.org/10.1061/\(ASCE\)1090-0241\(2004\)130:9\(975\)](https://doi.org/10.1061/(ASCE)1090-0241(2004)130:9(975))
- Yasuda, S. et al. (1999) 'Effect of degree of saturation on the liquefaction strength of Masa', in *34th Japanese National Conference Geotechnical Engineering*, pp. 2071–2072.
- Yegian MK et al (2007) Induced-partial saturation for liquefaction mitigation: experimental investigation. *J Geotechnical Geoenviron Eng* 133(4):372–380. [https://doi.org/10.1061/\(ASCE\)1090-0241\(2007\)133:4\(372\)](https://doi.org/10.1061/(ASCE)1090-0241(2007)133:4(372))
- Yoshimi Y, Tanaka K, Tokimatsu K (1989) Liquefaction resistance of a partially saturated sand. *Soils Found* 29(3):157–162
- Zeybek, A. and Madabhushi, S. P. G. (2016) 'Centrifuge testing to evaluate the liquefaction response of air-injected partially saturated soils beneath shallow foundations', *Bulletin of Earthquake Engineering*. Springer Netherlands, pp. 1–18. doi: <https://doi.org/10.1007/s10518-016-9968-6>.
- Zeybek A, Madabhushi GSP (2017a) Durability of partial saturation to counteract liquefaction. *Proc Inst Civ Eng Ground Improv* 170(2):102–111. <https://doi.org/10.1680/jgrim.16.00025>
- Zeybek A, Madabhushi SPG (2017b) 'In fl uence of air injection on the liquefaction-induced deformation mechanisms beneath shallow foundations', *Soil Dynamics and Earthquake Engineering*. Elsevier Ltd 97(February):266–276. <https://doi.org/10.1016/j.soildyn.2017.03.018>
- Zeybek A, Madabhushi GSP, Pelecanos L (2020) 'Seismic response of partially saturated soils beneath shallow foundations under sequential ground motions', *Bulletin of Earthquake Engineering*. Springer, Netherlands 18(5):1987–2002. <https://doi.org/10.1007/s10518-020-00792-5>

Publisher's Note Springer Nature remains neutral with regard to jurisdictional claims in published maps and institutional affiliations.